Measurement of Speed of Light by Coincidence Count Method

Randy Stefan Tanuwijaya,* Tsz Kit Yung,† and Jensen T.H. Li‡
Department of Physics
The Hong Kong University of Science and Technology
Clear Water Bay, Hong Kong
(Dated: December 9, 2020)

The speed of light had been a lingering problem in Physics until the last century before the time-of-flight interferometry technique was established. Nowadays, there are various methods to measure the speed of light. Here, we demonstrate the speed of light measurement by analyzing the shift of coincidence count of incident photons by using a Single-Photon Avalanche-Diode Camera. The coincidence count is measured by using a 32x32-pixels picosecond-resolved camera, which is able to resolve the arrival time of photons within 55ps. This experiment serves as one of the calibration and preparation of future experiments in the quantum regime, particularly to verify the Hong-Ou-Mandel (HOM) effect.

I. INTRODUCTION

The first realization and attempt to measure the speed of light can be traced back to 1676, by Danish astronomer Ole Roemer, by observing the eclipse Io, one of the satellites of Jupiter [1]. Afterwards, around the 19-th century, the time-of-flight techniques emerge, in which utilizes interferometry to accurately measure the speed of light. The famous Michelson-Morley interferometer is one of the examples [2]. Since 1983, the metre is defined as "the length of the path travelled by light in vacuum during the time interval of $1/299\,792\,458$ of a second", and consequently fixing the definition of speed of light at $299\,792\,458$ m/s [3].

Nowadays, there are various methods to measure the time-of-flight. For example, one can measure the speed of light with $\sim$ 1% error by using an oscilloscope with nanosecond time resolution. Here, we will utilize the Time-Correlated Single-Photon-Counting (TCSPC) technique and by counting the coincidence count to measure the speed of light. TCSPC is a technique to measure the arrival time of a single photon within a clock cycle. The main component of TCSPC is the Single Photon Avalanche Diode (SPAD), which will convert the incidence photon into the electric detection signal. Array of SPADs with it's high temporal resolution has been previously utilized throughout many field in optics, such as fluorescence lifetime imaging [4], imaging through scattering media [5], imaging light in flight [6]. For this technique, we are using SPAD Camera (Photon Force PF32), a 32x32 TCSPC pixel array with 55ps time resolution to measure the speed of light.

* rstanuwijaya@connect.ust.hk
† tkyungaa@connect.ust.hk, postgraduate supervisor
‡ jensenli@ust.hk, faculty supervisor

II. TECHNICAL BACKGROUND

A. Single Photon Avalanche Diode (SPAD) in PF32

Avalanche diode which operates at biased voltage V_A above breakdown voltage V_B in Geiger mode of connected with avalanche-quenching circuit can be used to detect single photons [7]. This configuration is called SPAD. In this mode, a incident photon on the active area of the avalanche diode will trigger a detection signal. There are some characteristics of SPAD that is important to note, such as the photon detection efficiency, dark count rate (DCR), and instrument response function (IRF)/jitter.

The Figure 1 illustrates the photon detection probability or the quantum efficiency of SPAD in PF32. Photon detection probability corresponds to the probability of the incidence photon converted into electric detection signal. Other than the photon wavelength, the photon detection probability is also a function of the bias voltage.

The DCR is a function of temperature and bias voltage. The increase of temperature and bias voltage will effectively increases the DCR. Moreover, the electronic noise of the neighboring SPAD/cross-talk also affects the DCR. Cross-talk is caused because the avalanche process of the SPAD will emit some photons during the large flow of current. However, because of the large distance between each active areas, this effect is negligible.

Finally, the IRF and jitter is also important to note. IRF is the time required to convert the photon into the electric signal, and jitter is the variation of IRF within the different SPADs on the camera. Because of the difference in the manufacturing process, the jitter of each pixels is slightly different and calibration process is needed to determine the jitter of each individual pixel. Fortunately, even though the there is significant jitter among the pixels, the jitter is constant for each experiment. Therefore, once the jitter is calibrated, we can simply subtract the arrival time of the photons with the jitter of the corre-

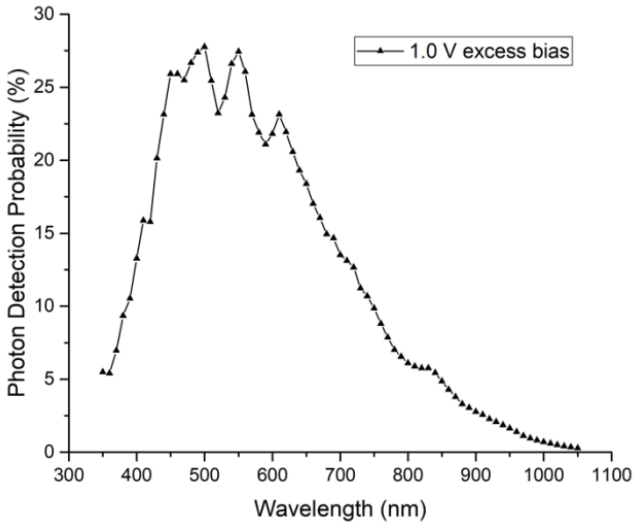

FIG. 1: Photon detection probability vs. wavelength of SPAD in PF32 obtained from the PF32 manual [8]

sponding pixel. More details about the jitter calibration will be discussed in the next section.

B. TCSPC Mode of PF32

The detection of single photon is performed by Single-Photon Avalanche Diode (SPAD) within each pixels of PF32. The TCSPC mode will mark the detection signal of the SPAD with a timestamp corresponding to the arrival time of the photon. The forward start-stop process of TCSPC can be thought of as a fast stopwatch, where it starts the time measurement at the emission of the pulsed light source, and stop the measurement at the detection of a single photon. Similar to many TCSPC systems, the PF32 performs reverse start-stop measurements, the detection of a single photon starts the time measurement and the next synchronisation pulse stops the process. The diagram in Figure 2 illustrates the TCSPC cycle in PF32.

The reverse start-stop diagram in Figure 2 can be understood as following. The laser beam passes through a diffuser and illuminates two surfaces, A and B. Photon are scattered from the surfaces will be collected by PF32. The surface A is located closer to the laser source, and the photon from surface A (tA_r) will be collected earlier compared to photon from surface B (tB_r) in reverse start-stop process. The photon detection will trigger the measurement cycle, and the next sync pulse will stop the measurement. The result of reverse start-stop process is the time stamp for surface A (tA_r) being of a greater value compared to the surface B (tB_r). The reverse start-stop are advantageous since the electronics are only active when a photon is being detected.

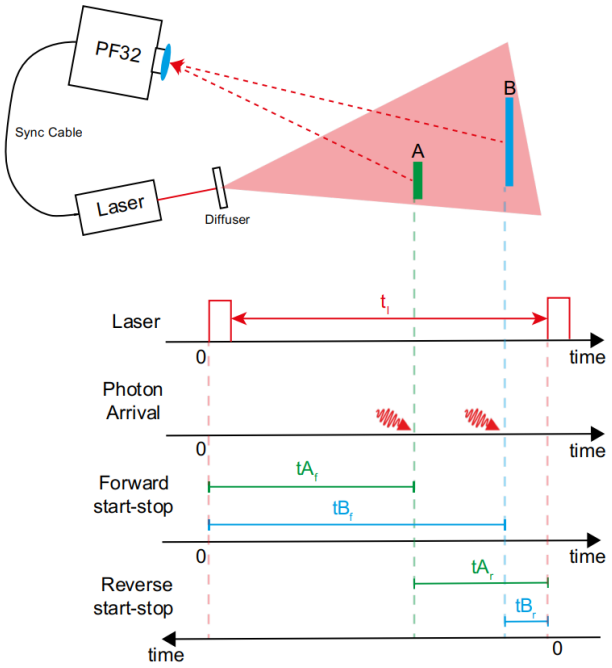

FIG. 2: Diagram of TCSPC cycle in PF32 obtained from the PF32 manual [8]

III. RESULTS

A. Experimental Setup

The setup for our experiment is illustrated in Figure 3. A pulsed white laser with frequency of 20 MHz along with a neutral-density (ND) filter and a monochromator at (632 ± 3) nm is used as the photon source in this experiment. The photodiode is used to sync the laser and the camera. The following path is the Mach-Zehnder interferometer. The light is passed to the beam splitter (BS) and split into two lines. The right and bottom line is the reference line, where the laser beam is reflected by an SLM (SLM is set to act as an mirror in this experiment). The top and left line is the delayed line, where we will use mirrors mounted on a motor to adjust the delay distance. The delay line scanning range is 200 mm, with 7 mm step. Finally, the path will be recombined at the second BS and can be imaged by the camera as two spots. The camera is operated in TCSPC mode with 5 s acquisition time.

B. Data Processing

The data processing is required to calculate the coincidence count from the raw data (arrival time of the photons for each pixel). First, we start by filtering the bad pixels and considering the jitter of each pixel. The jitter calibration has been done prior to this experiment, where we measure the jitter time for each pixels. The

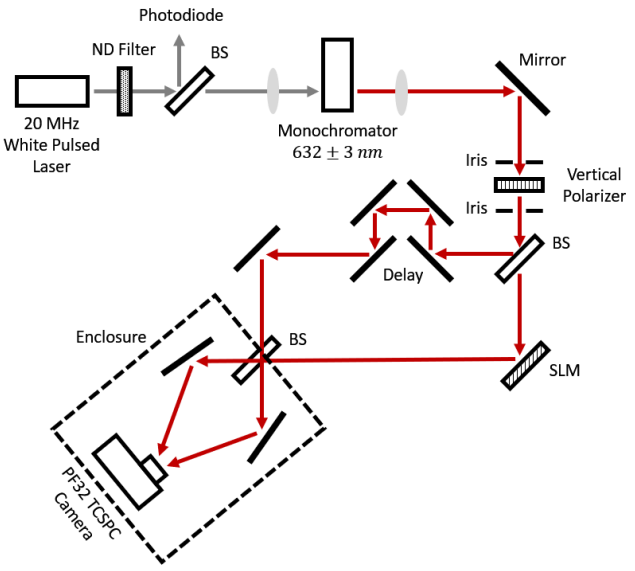

FIG. 3: Experimental Setup of the speed of light measurement. The laser is split into two lines, the reference and the delayed line, and later recombined and detected by the TCSPC camera.

measured average jitter time is 102 ps and with standard deviation of 155 ps. For jitter calibration, we simply subtract the raw data with the jitter of each pixels.

Figure 4a (left) shows the raw photon count for each pixels. As we can see, the raw data includes some bad pixels. Figure 4a (right) shows the photon count after excluding the bad pixels. Figure 4b shows the jitter of each pixels, with units in the size of time bin, (53.42 ± 0.30) ps.

The main part of the data processing is counting the coincidence. First, we define two region of interest at the same spot, marked in red at Figure 4a (right). Here we choose the region of interest to be the brightest area on the left spot. Choosing the region of interest from the one spot is sufficient because each spot is composed of the light from the reference and the delayed line. We define the coincidence count for each time difference, $C(\Delta t)$ as the number of photon arriving at the different region of interest with the time difference Δt. Figure 5 shows the coincidence counts for some delay line positions. Then, we fit the data by using multiple Lorentzian fit to find the center and off peaks temporal positions. The central peak corresponds to the coincident photon arriving from the same line, i.e. both photons from the reference or delayed line. The off peaks correspond to the photon arriving from the different line, and the peak position corresponds to the time-of-flight of the photons. Finally, Figure 6 shows the linear fit of the off peaks at different delay line positions. Note that some data points are excluded when the off peaks are too close to the center peak and become indistinguishable. The slope of the linear fit corresponds to the speed of light, where:

$$m = -\frac{2}{c_m} \iff c_m = (3.081 \pm 0.019) \times 10^8 \,\mathrm{m/s} \quad (1)$$

where m is the slope of the off peak positions and c_m is the measured speed of light

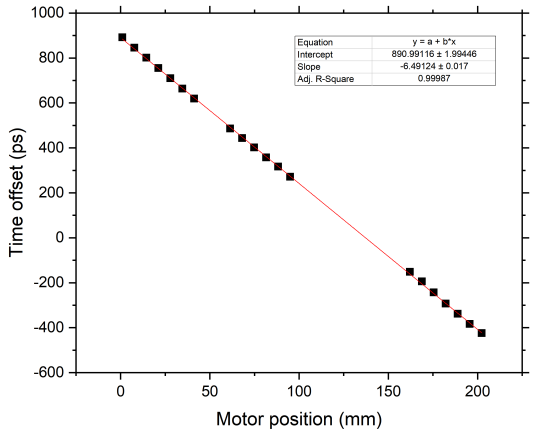

FIG. 6: Linear fit of the off peaks, with obtained speed of light $c_m = (3.081 \pm 0.019) \times 10^8$ m/s

C. Discussion

The result obtained in this experiment does not agree with the speed of light $c = 2.998 \times 10^8$ m/s with discrepancy of 2.7%. Other factors that contribute to the error but ignored in this experiment are temperature, humidity, and air refractive index. One of the possible extensions of this experiment is to measure the refractive index of a material. Moreoever, this setup can be adjusted easily to other experiments that utilizes Mach-Zehnder interferometry.

IV. CONCLUSION

This experiment demonstrates the capability of measuring the speed of light at low-intensity events, in contrast to the commonly used interferometry methods. More importantly, it shows the promising capability of the SPAD camera for the future experiments, such as quantum optics experiment. In fact, the experimental setup is designed specifically this way to be easily transitioned to one of the quantum optical experiments, which is to verify the Hong–Ou–Mandel effect. The Hong-Ou-Mandel effect requires interference of light at the beam splitter at very low light intensity, with random phase initialization. For this reason, we used an additional beam splitter and included the SLM in our experimental setup, rather than simply measuring the time difference

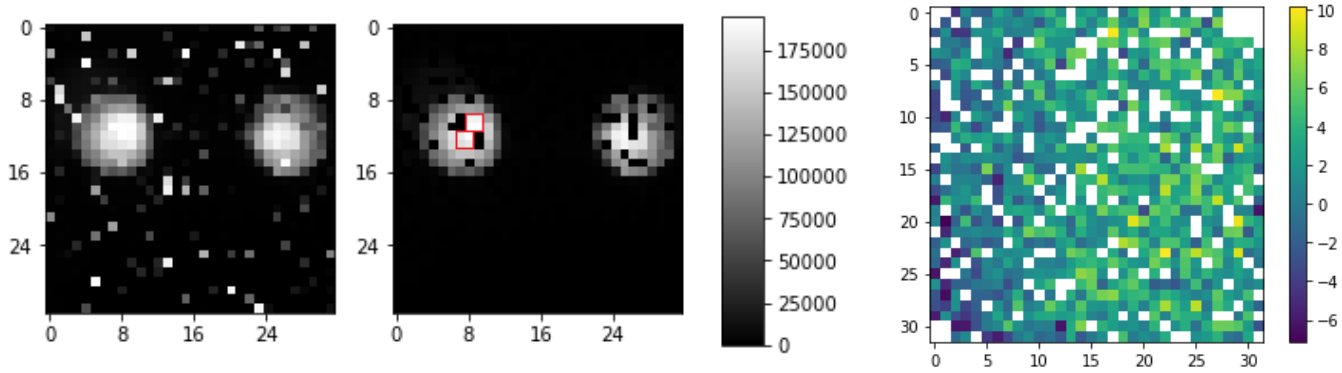

(a) Photon Count before (left) and after (right) removal of bad pixels, region of interests marked with red square

(b) Variation of jitter of the pixels, bad pixels marked in white

FIG. 4: Calibration process of the data

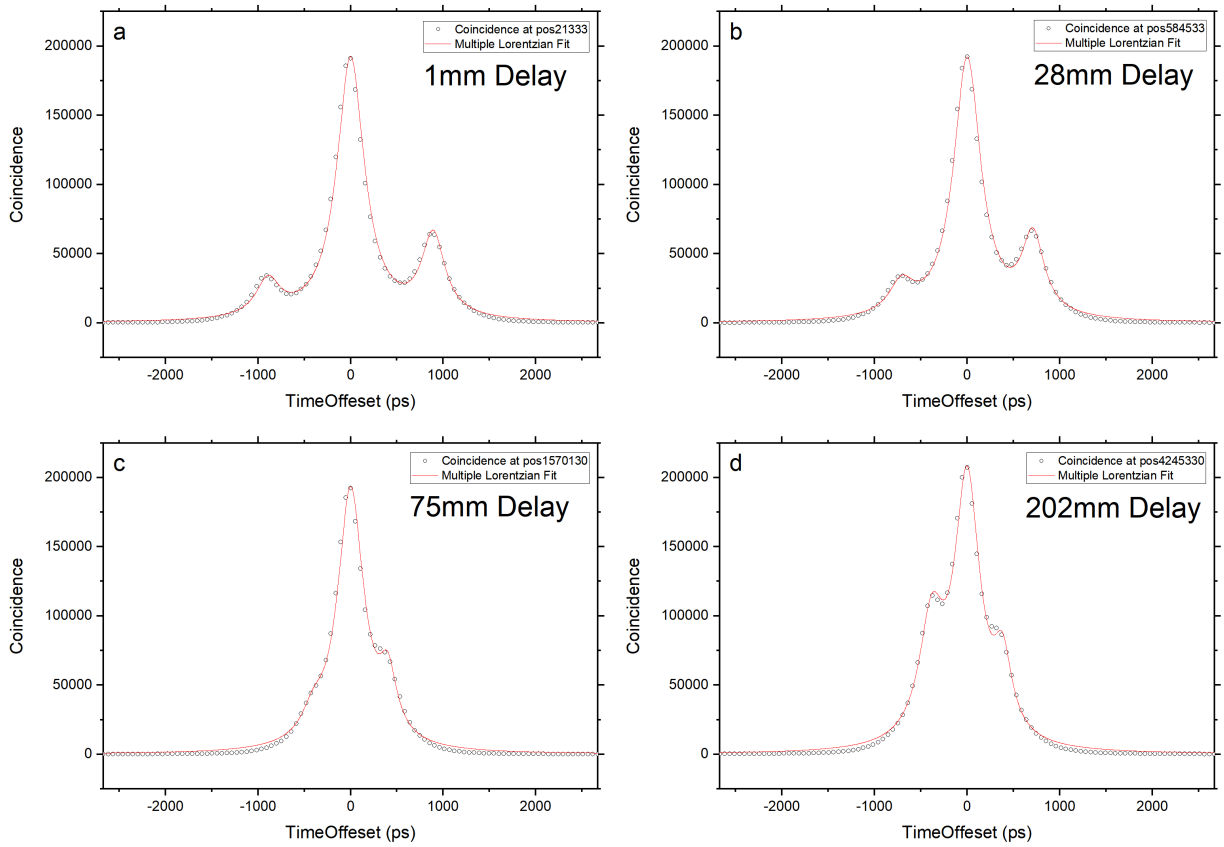

FIG. 5: Coincidence count at different delay line positions

between two independent light spots. This simple experiments demonstrates many possibilities of the future experiments.

[1] M. Roemer and I. B. Cohen, Roemer and the first determination of the velocity of light, Isis **31**, https://doi.org/10.1086/347594 (1940).

[2] A. A. Michelson, Measurement of the velocity of light between mount wilson and mount san antonio, The Astrophysical Journal **65**, 1 (1927).
[3] (1983).
[4] S. P. Poland, N. Krstajic, J. Monypenny, S. Coelho, D. Tyndall, R. J. Walker, V. Devauges, J. Richardson, N. Dutton, and P. e. a. Barber, A high speed multifocal multiphoton fluorescence lifetime imaging microscope for live-cell fret imaging, Biomedical Optics Express **6**, 277 (2015).
[5] G. Satat, M. Tancik, O. Gupta, B. Heshmat, and R. Raskar, Object classification through scattering media with deep learning on time resolved measurement, Optics Express **25**, 17466 (2017).
[6] G. Gariepy, N. Krstajic, R. Henderson, C. Li, R. R. Thomson, G. S. Buller, B. Heshmat, R. Raskar, J. Leach, and D. Faccio, Single-photon sensitive light-in-fight imaging, Nature Communications **6**, 10.1038/ncomms7021 (2015).
[7] S. Cova, M. Ghioni, A. Lacaita, C. Samori, and F. Zappa, Avalanche photodiodes and quenching circuits for single-photon detection, Applied Optics **35**, 1956 (1996).
[8] P. Force, *PF32 User Manual*, v1.5.14 (2020).